A CCD Study of High Latitude Galactic Structure: Testing the Model Parameters

S. Karaali, ^{1,2} S. G. Ak, ¹ S. Bilir, ¹ Y. Karataş ¹, and G. Gilmore ³

- ¹Istanbul University Science Faculty, Department of Astronomy and Space Sciences, 34452 University-Istanbul, Turkey
- ²Visiting Astronomer, Institute of Astronomy, Madingley Road, Cambridge, CB3 OHA, UK
- ³Institute of Astronomy, Madingley Road, Cambridge, CB3 OHA, UK

Accepted 2002 month day. Received year month day;

ABSTRACT

We interpret published CCD UBVI data to deduce the stellar density distribution and metallicity distribution function in the region from 2-8 kpc from the Galactic Plane, and compare our results to several star count models. A feature of extant star count models is degeneracy between the adopted scale heights of the thin and thick disks, and their local normalisation. We illustrate the utility of this small data set, and future larger sets (e.g. SDSS), by explicitly considering consistency between the derived density laws, and the implied solar neighbourhood luminosity function. Our data set, from Hall et al. (1996) ($l=52^o,b=-39^o$) contains 566 stars, selected to be consistent with stellar loci in colour-colour diagrams. The effective apparent V-magnitude interval is $15.5 \le V_o \le 20.5$. Our analysis supports the parameterisation of the recent (SDSS) galaxy model of Chen et al. (2001), except in preferring the stellar halo axis ratio to be $\eta=0.84$.

Photometric metal-abundances have been derived for 329 stars with $(B-V)_o \leq 1.0$ using a new calibration. This show a multimodal distribution with peaks at [Fe/H]=-0.10, -0.70, and -1.50 and a tail down to -2.75 dex. The vertical distance-dependent metallicity distribution function, if parameterised by a single mean value, can be described by a metallicity gradient $d[Fe/H]/dz \sim -0.2$ dex/kpc for the thin disk and thick disk, and $d[Fe/H]/dz \sim -0.1$ dex/kpc for the inner halo, to z=8 kpc. The data are however better described as the sum of three discrete distribution functions, each of which has a small or zero internal gradient. The changing mix of thin disk, thick disk and halo populations with distance from the plane generates an illusion of a smooth gradient.

Key words: Galaxy: abundances – Galaxy: models – Stars: luminosity function.

1 INTRODUCTION

The traditional star count analyses of Galactic structure have provided a picture of the basic structural and stellar populations of the Galaxy. Examples and reviews of these analyses can be found in Bahcall (1986), Gilmore et al. (1989), Majewski (1993), Robin et al. (2000), and recently in Chen et al. (2001). The largest of the observational studies prior to SDSS are based on photographic surveys; the Basle Halo Program (Becker 1965) has presented the largest systematic photometric survey of the Galaxy (Fenkart 1989a, b, c, d; Del Rio & Fenkart 1987; Fenkart & Karaali 1987; Fenkart & Karaali 1990; Fenkart & Karaali 1991). The Basle Halo Program photometry is currently being recalibrated and reanalysed, using an improved calibration of the RGU photometric system (Buser et al. 1998, 1999; Ak et al. 1998; Karataş et al. 2001). More recent and future studies are being based on CCD survey data. Most have in general much smaller area coverage or a restriction to only high Galactic latitudes, or a focus at faint magnitudes (e.g.

Willman et al. 2002; Chen et al. 2001). HST studies are a limiting case (e.g. Johnson et al. 1999), with very deep but extremely small area coverage, and corresponding very poor statistical weight. The general absence of CCD *UV* data additionally makes such analyses sensitive to assumptions on metallicity distributions.

Even small-area CCD studies probing intermediate apparent magnitudes can be valuable, however, when analysed in the light of known solar neighbourhood constraints, especially consistency with the local stellar luminosity function. This is required since star-count analyses are essentially an attempt to deconvolve the product of a density profile and a local normalisation, with that local normalisation being the solar neighbourhood luminosity function for the specific stellar population of relevance. The local luminosity function determined from Hipparcos parallax data and that deduced from star count analyses must be consistent, providing an additional constraint on Galactic modelling, or an independent check on photometric calibrations. Here we illustrate this consis-

tency by analysing the small area 5-colour *UBVRI* CCD survey by Hall et al. (1996).

We do not here use the available SDSS data, partly since these have recently been analysed by Chen etal, but alos since our aim is to illustrate the general approach. Over the next few months massive photometric data sets will become available from SDSS, 2MASS, DENIS, UKIDSS, VST, CFH/Megacam, Suprime,.... These data sets will combine statistical weight with the wide area coverage which will allow consideration of second-order effects, quantifying the structure of the Galaxy beyond simple analytic smooth functions. Given that, it is timely now to consider method, rather than specific interim results.

In addition to a direct test of the density profile/luminosity function consistency requirements, we use the information available in the multi-colour photometry, especially the U-band data, to derive limits on metallicity gradients in the thin disk, thick disk, and halo.

The existence of a clear vertical metallicity gradient for any pressure-supported component of the Galaxy means that it formed by dissipative collapse. The pioneers of this suggestion are Eggen, Lynden-Bell, & Sandage (1962 hereafter ELS) who argued that the Galaxy collapsed in a free-fall time ($\sim 2x10^8$ yr). A discussion of the current status of this model is provided by Gilmore, Wyse & Kuijken (1989). Over the past 20 years, observational studies have revealed that the collapse of the Galaxy occurred slowly with the limiting case being assembly of the Galaxy on many dynamical times, which (now allowing for a dark matter halo), implies times of very many Gyr (e.g. Yoshii & Saio 1979; Norris, Bessel & Pickles 1985, hereafter NBP; Norris 1986; Sandage & Fouts 1987; Carney, Latham & Laird 1990; Norris & Ryan 1991; Beers & Sommer-Larsen 1995). This picture was postulated largely on a supposed wide age in the globular cluster system (Searle & Zinn 1978, hereafter SZ; Schuster & Nissen 1989). SZ especially argued that the Galactic halo was not formed in an ordered collapse, but from merger or accretion of numerous fragments, such as dwarftype galaxies. Such a scenario indicates no metallicity gradient or young and even more metal-rich objects at the outermost part of the Galaxy. The globular cluster age range supposition has been disproved by recent analyses (Rosenberg et al. 1999), while the number of young field halo stars has been shown to be extremely small, inconsistent with the model, by Unavane, Wyse & Gilmore (1996) and Preston & Sneden (2000, see also Gilmore 2000). Nonetheless, hierachical models have become the default (Freeman & Bland-Hawthorn 2002). We readdress the metallicity gradient from the present data.

In Section 2, we describe the selection of the sample (566 stars) from the 4462 objects (stars, galaxies, quasars etc.) observed by Hall et al. (1996), separation of the sample stars into different populations, and their absolute magnitude determination. Section 3 discusses the density functions, for seven absolute magnitude intervals evaluated for distances beyond $r=0.4~\rm kpc$, with three galactic models and comparison of the resulting luminosity functions with that of Hipparcos (Jahreiss & Wielen 1997) and Gliese & Jahreiss (1992). In Section 4, we search for a metallicity gradient in each of the galactic components, i.e.: thin disk, thick disk, and halo. Section 5 provides a summary and discussion. Finally, a summary is given for the new calibration in an appendix.

Figure 1. Two-colour diagrams for 922 objects with stellar image profiles from Hall et al. (1996). (a) for $(U-B)_o$ versus $(B-V)_o$, and (b) for $(V-I)_o$ versus $(B-V)_o$. Objects with $(U-B)_o < -0.46$ mag, corresponding to $(u'-g')_o < -0.5$ mag in the Sloan photometry are extra-galactic objects

Figure 2. Two-colour diagrams for objects with $(U-B)_o \geq -0.46$ and $V_o \leq 20.5$. (a) for $(U-B)_o$ versus $(B-V)_o$, and (b) for $(V-I)_o$ versus $(B-V)_o$. The U-B selection has reduced the scatter relative to that in Fig.1a and b.

2 DATA

2.1 Star-Galaxy-QSO separation

i.e.: A(V) = 3.1E(B - V).

The data are taken from the catalogue of Hall et al. (1996), who provide a deep multi-colour survey for 12 CCD fields. From the 4462 sources they detected, we selected the stellar-like sources labelled with "s", "sf", "Fs" in the catalogue for Field 21e-w (Galactic coordinates $l=52^{o}$, $b=-39^{o}$, area 0.149 square degree). We adopted the mean of two E(B-V) colour-excesses given by Hall et al. (1996), i.e.: 0.0223 mag, for all stars and we de-reddened U-B and V-I colour-indices by the following well known equations:

$$E(U-B) = 0.72E(B-V) + 0.05E^{2}(B-V)$$
 (1)
$$E(V-I) = 1.250[1 + 0.06(B-V)_{o} + 0.014E(B-V)]E(B-V)(2)$$
 the total absorption $A(V)$ is evaluated as usual,

We restricted the sample at the faint end, corresponding to the peak in the distribution of apparent magnitudes, at $V_o=20.5$ mag, leaving 922 sources. The two-colour diagrams $(U-B)_o - (B-V)_o$ and $(B-V)_o - (V-I)_o$, for these objects indicate residual significant contamination by extra-galactic objects (galaxies and QSO) and, WD and BHB stars (Fig.1a and b). We then rejected all sources with $(U-B)_o < -0.46$, which corresponds to the location of the bluest extra-galactic objects, $(u'-g')_o < -0.5$ mag, in SDSS (Chen et al. 2001). This (U-B) cut removed most outliers in the (BVI) two-colour diagrams (Fig.2). We further removed those few sources which lay significantly off the stellar locus in (UBVI), limiting the sample to 566 sources with stellar colours (Fig.3).

2.2 Stellar population types and absolute magnitude determination

The $(B-V)_o$ colour distribution of the sample stars shows a bimodal distribution (Fig.4), as expected for a high-latitude field (see, e.g. Phleps et al. 2000). In order to assign (statistical) distances, we need to distinguish (statistically) between the three basic metallicity-dependent populations, thin disk, thick disk and halo. It is well known (cf Chen et al. (2001) for a recent discussion) that population types are a complex function of both colour and apparent magnitude. According to Chen et al., the halo has a turnoff at $(g'-r')_o=0.20$ mag and it dominates in the apparent magnitude interval fainter than $g'_o\sim18$ mag, whereas the thick disk has a turnoff at $(g'-r')_o=0.33$ mag and it is dominant at brighter apparent magnitudes, $g'_o<18$ mag. The corresponding turnoff

Figure 3. Two-colour diagrams for the final sample after excluding outliers in Fig.2a and b. (a) for $(U-B)_o$ versus $(B-V)_o$, and (b) for $(V-I)_o$ versus $(B-V)_o$.

Table 1. The colour-magnitude intervals most appropriate for statistical discrimination of the three stellar populations.

Populations V_o	Thin Disk $(B-V)_o$	Thick Disk $(B-V)_o$	Halo $(B-V)_o$
(15.5-16.0]	≥ 0.9	< 0.9	_
(16.0-17.0]	≥ 0.9	< 0.9	
(17.0-18.0]	≥ 0.9	< 0.9	_
(18.0-19.0]	≥ 1.0	[0.5 - 1.0)	< 0.5
(19.0-20.0]	≥ 0.9	_	< 0.9
(20.0-20.5]	≥ 0.9	_	< 0.9

Figure 4. Colour distribution for 566 stars in our sample. The thin disk population, $(B-V)_o>1.0$ mag, is rather conspicuous whereas thick disk and halo populations, $(B-V)_o<1.0$, overlap.

colours in the UBVRI system are $(B-V)_o=0.41$ and 0.53 mag for halo and thick disk, respectively. The diagram V_o versus $(B-V)_o$ in Fig.5 reveals these three populations, with, for example, the blue shift of the turnoff moving from thick disk to halo being apparent near V=18. It seems that thick disk and halo populations overlap in Fig.4. Hence, the colour distribution of the sample stars is given as a function of apparent magnitude (Fig.6) and the turnoffs for thick disk and halo, as well as for thin disk, are fixed precisely (Table 1).

Assignment of individual absolute magnitudes for stars classified into the different populations are determined by means of appropriate colour-absolute magnitude relations, as follows. The M(V) absolute magnitudes and $(B-V)_o$ of Lang (1992) are used to define the colour-absolute magnitude relation for thin disk stars (Fig.7a). The colour-absolute magnitude relation for thick disk stars is adopted from the globular cluster 47 Tuc ([Fe/H] $\,=\,-0.65$ dex), with data taken from Hesser et al. (1987). These authors provide V and B - V data as well as E(B - V) colour excess (0.04) mag) and apparent distance modulus, V - M(V) = 13.40 mag, which gives the absolute magnitude of a star by combination with the total absorption, A(V) = 3.1E(B - V) (Fig.7b). For the halo, we used two colour-absolute magnitude relations, that for the globular cluster M13 ([Fe/H] = -1.40 dex) for stars with $(B-V)_o \ge$ 0.40 mag and that of the globular cluster M92 ([Fe/H] = -2.20dex) for only an interval less than one magnitude which is not covered by the diagram of M13 (0.30 $< (B - V)_o \le 0.40$). We applied the same procedure as noted above for the calibration of 47 Tuc, to the data of Richer & Fahlman (1986) and Stetson & Harris (1988). Richer & Fahlman provide E(B-V)=0.02 mag and V - M(V) = 14.50 mag for M13, while Stetson & Harris give E(B-V) = 0.02 mag and V-M(V) = 14.60 mag for M92. The colour-absolute magnitude relations for M13 and M92 are given in Fig.7c and d.

Figure 5. V_o versus $(B-V)_o$ diagram for the sample stars. Contrary to the distribution in Fig.4, thick disk and halo stars can be distinguished, with, for example, the appearance of a blue halo turnoff being apparent near $V_o=17.5,\,(B-V)_o=0.4$.

Figure 9. The stellar luminosity functions, at r=0 kpc, resulting from comparisons of derived space densities with galactic models, (a) Gilmore & Wyse (1985), (b) Buser, Rong & Karaali (1999), and (c) Chen et al. (2001), compared to that of Hipparcos (Hip 1997), and Gliese & Jahreiss (GJ 1992).

Figure 10. The stellar luminosity function, at r=0 kpc, resulting from comparisons of derived space densities with the galactic model of Chen et al. (2001), with some modifications. In (a) and (b) the axis ratio for the halo is adopted as 0.65 and 0.84 respectively, and in (c) the density law for the halo is assumed to be de Vaucouleurs instead of power-law (with axis ratio 0.84). Comparison of these luminosity functions with that of Hipparcos (Hip 1997), and Gliese & Jahreiss (GJ 1992) favours the models in the lower two panels.

3 DENSITY FUNCTIONS AND LUMINOSITY FUNCTION

The logarithmic space densities $D^* = log D + 10$ are evaluated for stars for seven absolute magnitude intervals, i.e.: $4 < M(V) \le 5$, $5 < M(V) \le 6$, $6 < M(V) \le 7$, $7 < M(V) \le 8$, $8 < M(V) \le 9$, $9 < M(V) \le 10$, and $10 < M(V) \le 11$ mag, over the distance range for which absolute magnitudes are completely sampled by the available photometry (Table 2). The number of stars brighter than M(V) = 4 is also given in the same table. Here, $D = N/\Delta V_{1,2}$, N being the number of stars, found in the volume $\Delta V_{1,2}$, which is determined by its limiting distances r_1 and r_2 and by the apparent field-size in square degrees \Box , i.e.: $\Delta V_{1,2} = (\frac{\pi}{180})^2 (\frac{\Box}{3}) (r_2^3 - r_1^3)$.

The density functions are most conveniently presented in the form of histograms whose sections with ordinates $D^*(r_1, r_2)$ cover the distance-intervals (r_1, r_2) . Heavy dots on the histogram sections $D^*(r_1, r_2)$ designate the centroid-distance $r^* = [(r_1^3 +$ $(r_2^3)/2$ of the corresponding partial volume $\Delta V_{1,2}$ (Del Rio & Fenkart 1987; Fenkart & Karaali 1987; Fenkart 1989a, b, c, d). The density functions are compared with three galactic models, i.e.: Gilmore & Wyse (1985, hereafter GW); Buser, Rong, & Karaali (1998, 1999; hereafter BRK); and Chen et al. (2001, hereafter C) given in the form $\Delta log D(r) = log D(r, l, b) - log D(0, l, b)$ versus r, where $\Delta log D(r)$ is the logarithmic difference of the densities at distances r and at the Sun. Thus, $\Delta log D(r) = 0$ is the logarithmic space density at r = 0, which is the parameter required for luminosity function determination. The comparison is carried out as explained in several studies of the Basle fields (Del Rio & Fenkart 1987; Fenkart & Karaali 1987), i.e.: by shifting the model curve perpendicular to the distance axis until the best fit to the histogram results at the centroid distances. Fig.8 shows the comparison of the observed density functions with the model BRK as an example.

There is adequate agreement between both models and the observed density functions within the limiting distance of completeness marked by horizontal thick lines in Table 2. However, this is not the case when one includes the luminosity functions. As cited above, the luminosity function close to the Sun: $\varphi^*(M)$, i.e.: the logarithmic space density for the stars with M±0.5 mag at r=0 is the D^* -value corresponding to the intersection of the model-curve with the ordinate axis of the histogram concerned. The luminosity functions resulting from comparisons of our space density data with the models GW, BRK, and C confronted to the luminosity function of Hipparcos (Jahreiss & Wielen 1997) and that of Gliese & Jahreiss (GJ 1992) are given in Fig.9a, b, and c, respectively.

When we compare the luminosity functions obtained in this work with the luminosity function from Hipparcos, the Buser et

4 Karaali et al.

Figure 6. Colour distributions for 566 stars in our sample as a function of apparent magnitude. The colour limits revealed from these panels which allow sub-population isolation are given in Table 1.

Figure 7. $M(V) - (B - V)_o$ colour-absolute magnitude relations for three populations. (a) for thin disk, (b) for thick disk, and (c) and (d) for halo (see text for details).

Figure 8. Comparison of logarithmic space densities with the galactic model of BRK for (a) $4 < M(V) \le 5$, (b) $5 < M(V) \le 6$, (c) $6 < M(V) \le 7$, (d) $7 < M(V) \le 8$, (e) $8 < M(V) \le 9$, (f) $9 < M(V) \le 10$, and (g) $10 < M(V) \le 11$ mag. Heavy dots designate the centroid-distance $r^* = [(r_1^3 + r_2^3)/2]^{1/3}$ of the corresponding partial volume $\Delta V_{1,2}$.

Table 2. Logarithmic space densities, $D^* = logD + 10$ for seven absolute magnitude intervals, where $D = N/\Delta V_{1,2}$, N being the number of stars, found in the partial volume $\Delta V_{1,2}$, which is determined by its limiting distances r_1 and r_2 and by the apparent field - size in square degrees \Box ; i.e.: $\Delta V_{1,2} = (\frac{\pi}{180})^2 (\frac{\Box}{3})(r_2^3 - r_1^3)$. $r^* = [(r_1^3 + r_2^3)/2]^{1/3}$: centroid-distance of the partial volume $\Delta V_{1,2}$. Two thick horizontal lines for each absolute magnitude interval define the distance interval for completeness (distances in kpc, volumes in pc^3).

		$M(V) \!\!\to\!\!$	(2-3]	(3-4]	(4-5]	(5-6]	(6-7]	(7-8]	(8-9]	(9-10]	(10-11]
r_1 - r_2	$\Delta V_{1,2}$	r*	N D*	N D*	N D*	N D*	N D*	N D*	N D*	N D*	N D*
0.00- 0.40	9.54(02)	0.32							1 7.02	3 7.50	1 7.02
0.40- 0.63	2.85(03)	0.54						2 6.85	6 7.32	9 7.50	7 7.39
0.63- 1.00	1.13(04)	0.86				5 6.64	13 7.06	3 6.42	17 7.18	16 7.15	5 6.64
1.00- 1.59	4.51(04)	1.36			4 5.95	22 6.69	21 6.67	14 6.49	19 6.62	28 6.79	1 5.35
1.59- 2.51	1.80(05)	2.15			13 5.86	$27 \ 6.18$	44 6.39	26 6.16	25 6.14	4 5.35	
2.51- 3.98	7.15(05)	3.41			$\overline{13\ 5.26}$	25 5.54	27 5.58	19 5.42	3 4.62		
3.98- 6.31	2.85(06)	5.40			17 4.78	22 4.89	18 4.80	4 4.15			
6.31- 7.94	3.78(06)	7.22		2 3.72	9 4.38	7 4.27	4 4.02				
7.94-10.00	3.78(06)	9.09		3 3.60	12 4.20	3 3.60					
10.00-12.59	1.51(07)	11.44	1 –	2 3.12	10 3.82	7 3.67					
12.59-15.85	3.00(07)	14.40		3 3.00	6 3.30						
15.85-17.78	2.48(07)	16.87			3 3.08						
		Total	1	10	87	118	127	68	71	60	14

Table 3. Model parameters of Buser et al. (BRK 1998, 1999), Gilmore & Wyse (GW 1985), and Chen et al. (C 2001) and their comparison (fifth and sixth columns). Symbols: n_i (i = 0, 1, 2, 3) local density relative to thin disk, H_i (i = 0, 1, 2) scale-height in pc, h_i (i = 0, 1, 2) scale-lenght in pc, R_{eff} : effective radius in pc, R_{\odot} distance of the Sun to the Galactic center in pc, R_{\odot} axis ratio for halo, and R_{\odot} core radius in pc.

Authors	BRK	GW	С	BRK-GW	BRK-C
Thin Disk	Double Exponential	Double Exponential	Double Exponential	_	_
n_0	$0.2^{(1)}$	0.2	$0.2^{(1)}$	_	_
n_1	1.0	1.0	1.0	_	_
H_0	170	100	90	_	80
H_1	292.5	300	330	_	_
h_1	4010	4000	2250	_	1760
Thick Disk	Double Exponential	Double Exponential	Double Exponential	_	_
n_2	0.059	0.02	0.075	_	_
H_2	910	1000	750	90	160
h_2	3000	4000	3500	_	500
Halo	de Vaucouleurs	de Vaucouleurs	Power-law	_	_
n_3	0.0005	0.001	0.00125	_	_
R_{eff}	2696	2700	_	_	_
η	0.84	0.85	0.55	_	0.29
R_{\odot}	8600	8500	8600	_	_
Power-law index	_	_	2.5	_	_
r_c	_	_	1000	_	_

⁽¹⁾ adopted

al. (BRK) model is most successful for intrinsically bright stars, $M(V) \leq 8$ mag, whereas the model of Chen et al. fits the data better for intrinsically fainter stars, M(V) > 8 mag. Obviously, the reason for the difference in this comparison of effective local luminosity functions is due to the difference between the parameters used (Table 3). For the models of Gilmore & Wyse (GW) and of Buser et al. (BRK), the main difference is between the scale-height and local density of the thick disk, whereas for Buser et al. (BRK) and Chen et al. (C) the differences involve five parameters, i.e.: the scale-heights and scale-lengths of the thin and thick disks, and the axis ratio of the halo. The effect of the different density law (power-law) used for the halo in the model of Chen et al. will be discussed below

We modified the C-model of Chen et al. by changing the halo axis ratio from their adopted 0.55 to 0.65 and 0.84, respectively. The luminosity function resulting from comparison of this modified model with the observed density functions is in substantially improved agreement with the luminosity function of Hipparcos. This modified model matches the data better overall than does the Buser et al. BRK model (Fig. 10a and b). Now, a question arises from this comparison whether or not a power-law for the halo density matches the observations to the Galactic models better. We therefore recalculated the Chen et al. model, adopting a de Vaucouleurs spheroid denity law (with axis ratio 0.84) for the halo in place of the Chen et al. power-law. Comparison of this new model with the local normalisation data (Fig.10c) shows an improved fit, relative to the power-law model. Hence, regarding the best fit of the local luminosity function constraint resulting from comparison of the observed density functions for absolute magnitude intervals $4 < M(V) \le 5$, $5 < M(V) \le 6$, $6 < M(V) \le 7$, $7 < M(V) \le 8, 8 < M(V) \le 9, 9 < M(V) \le 10,$ and $10 < M(V) \le 11$, we conclude that the data suggest an increase in the axis ratio in the density law for the halo, to a value of $\eta = 0.84$, and further slightly prefer a halo density profile described by a de Vaucouleurs profile rather than a power-law.

4 METALLICITY DISTRIBUTION

The metal abundances for 329 stars with $(B-V)_o \leq 1.0$ mag were evaluated by means of a new calibration, of the standard metallicity-dependent ultraviolet-excess photometric parameter $\delta_{0.6}$, i.e.: $[Fe/H] = 0.10 - 2.76\delta - 24.04\delta^2 + 30.00\delta^3$, obtained via 88 dwarfs where the determination of abundances for most of them is based on high-resolution spectroscopy (Karaali et al. 2002). The metallicity distribution for the sample of all stars is multimodal (Table 4 and Fig.11g); one sees three local maxima, at [Fe/H] = -0.10, -0.70, and -1.50 dex, and a tail down to -2.75 dex.

However, one notices a systematic shift from the metal-rich stars to the metal-poor ones, when the distribution is considered as a function of apparent magnitude (Fig.11a-f). This is particularly apparent in Fig.12, where the mean metallicity as a function of z-distance is displayed. The overall distribution shows a continuous metallicity gradient d[Fe/H]/dz = -0.20 dex/kpc, up to z=8 kpc. It is interesting that the gradient is only marginally different for the thin disk (z<1.5 kpc) and thick disk (1.5<z<5 kpc), whereas the halo shows a weak, if not zero metallicity gradient between 5 and 8 kpc, i.e.: d[Fe/H]/dz = -0.10 dex/kpc, and zero at larger distances. At face value this indicates a continuous smooth vertical abundance gradient through the thick disk. However, this presentation assumes that a single parameter, the mean, is

Figure 12. Mean metal abundance versus mean z-distance for 10 z-intervals, suggesting a metallicity gradient $d[Fe/H]/dz \sim -0.2$ dex/kpc for the thin disk and thick disk, and $d[Fe/H]/dz \sim -0.1$ dex/kpc for the inner halo. As shown in the text, this apparent smooth abundance gradient is an artefact of a mix of three independent distributions.

adequate to describe a distribution function which is not gaussian, but is multi-modal. Is a single parameter a valid description of the data?

To consider this in more detail, the modes are evaluated (Table 4) for the metallicity distribution in figures 11a-11g, and the metallicity distributions are given for different z-intervals, z being the distance of a star to the Galactic plane in Table 5. The dips in Fig.11g separating three populations are statistically significant, for Hall et al. (1996) state that the external errors in their photometry as estimated from the two independent measurements of the magnitudes of each object, have been shown to be consistent with the internal errors computed according to photon statistics, except for an $\sim 2\%$ additional uncertainty independent of magnitude. This independent check proves that the flat-fielding process, aperture correction procedures, and photometry methods are all quite reliable, having inherent limitations of only the aformentioned $\sim 2\%$. As for systematic errors, their stellar locus matches values for stellar colours from the literature to about 5%. Three modes at [Fe/H] =-0.06, -0.83, and -1.59 dex for the distribution in Fig.11g correspond to the mean metal abundance for three components of the Galaxy, i.e.: thin disk, thick disk, and halo, though the one for the thick disk is a bit lower then the canonical one, [Fe/H] = -0.65dex, probably affected by the metal poor tail of the thick disk (Norris 1996, see section 5 for detail). The gaussians fits with the modes just cited and their sum are also shown in Fig.11g.

As figures 11a-11f makes clear, the apparent abundance gradient is evidently an artefact of the changing relative proportions of the three populations present, thin disk, thick disk, and halo, with each population having no significant gradient. Each abundance distribution is simply consistent with a sum of three discrete distributions, with no systematic change in the mode of each. This suggestion can be confirmed by the modes for individual apparent magnitude intervals (Table 4) which show fluctuations with exception the mode for the thick disk for the apparent magnitude interval 19 < V_o < 20, which is ~ -0.2 dex lower than the ones for brihter apparent magnitude intervals. This determination, with independent high-quality data and a new much improved photometric calibration, is essentially in agreement with the conclusions of Gilmore & Wyse (GW 1985): the Galactic disks are better described as the sum of independent well-mixed sub-populations with different spatial distributions than as a continuum. However, the mean metal abundance in Table 5 show a systematic decrease with increasing mean z, indicating a slight vertical metallicity gradient for thin disk, thick disk, and inner halo (see section 5 for detail).

5 SUMMARY AND DISCUSSION

In this work we illustrated the capabilities of present and forth-coming analyses of CCD star-count data, when such analyses are based purely on star by star inversion of colour data, through stellar photometric parallax. We showed how such analyses can be robust, provided that they utilise as a constraint consistency with the local solar neighbourhood stellar luminosity function. We showed how such analyses can limit possible metallicity gradients for the components of the Galaxy, and provide the choice of best model param-

6 Karaali et al.

Figure 11. Metallicity distribution for stars with $(B-V)_o \le 1.0$ mag as a function of apparent magnitude V_o (panels a-f), and for their combination within the limiting apparent magnitude, $V_o \le 20.5$ (last panel). (a) $15.5 < V_o \le 16$, (b) $16 < V_o \le 17$, (c) $17 < V_o \le 18$, (d) $18 < V_o \le 19$, (e) $19 < V_o \le 20$, (f) $20 < V_o \le 20.5$, and (g) $15.5 < V_o \le 20.5$. Curves in (g) are the fitted gaussians distributions for three populations (continuous curve) and their sum (dashed curve).

Table 4. Metallicity distribution for 329 stars of all apparent magnitudes (column 4) and for individual apparent magnitude intervals columns (5 -10), and the corresponding modes.

	$V_o \rightarrow$	(15.5-20.5]	(15.5-16.0]	(16-17]	(17-18]	(18-19]	(19-20]	(20.0-20.5]
[Fe/H](dex)	$<[Fe/H]>(\mathrm{dex})$	N	N	N	N	N	N	N
(-3.0) - (-2.8)	-2.9							
(-2.8) - (-2.6)	-2.7	1					1	
(-2.6) - (-2.4)	-2.5	2			1	1		
(-2.4) - (-2.2)	-2.3	5				3	2	
(-2.2) - (-2.0)	-2.1	9		1	1	1	4	2
(-2.0) - (-1.8)	-1.9	13				3	5	5
(-1.8) - (-1.6)	-1.7	14		1	1	5	6	1
(-1.6) - (-1.4)	-1.5	18			4	2	5	7
(-1.4) - (-1.2)	-1.3	11		1	1	5	3	1
(-1.2) - (-1.0)	-1.1	28	1	2	5	8	8	4
(-1.0) - (-0.8)	-0.9	28	3	2	3	7	10	3
(-0.8) - (-0.6)	-0.7	39	5	5	9	9	7	4
(-0.6) - (-0.4)	-0.5	21	2	4	6	5	3	1
(-0.4) - (-0.2)	-0.3	43	2	10	12	14	4	1
(-0.2) - (0.0)	-0.1	50	6	12	13	10	6	3
(0.0) - (+0.2)	+0.1	47	6	14	11	11	5	
	total	329	25	52	67	84	69	32
	mode 1	-0.06	0.00	+0.03	-0.13	-0.26	-0.07	
	mode 2	-0.83	-0.72	-0.65	-0.67	-0.73	-0.92	
	mode 3	-1.59			-1.50	-1.72	-1.70	

Table 5. Metallicity distribution for 329 stars for 10 z-distance intervals, z being the distance to the Galactic plane in kpc. Mean metal abundances and mean z distances, as well as mean errors for the metallicity are also indicated.

	$z(\mathrm{kpc}) \rightarrow$	(0-1]	(1-2]	(2-3]	(3-4]	(4-5]	(5-6]	(6-7]	(7-8]	(8-9]	(9-10]
[Fe/H](dex)	$<[Fe/H]>(\mathrm{dex})$	N	N	N	N	N	N	N	N	N	N
(-3.0) - (-2.8)	-2.9										
(-2.8) - (-2.6)	-2.7					1					
(-2.6) - (-2.4)	-2.5						1				
(-2.4) - (-2.2)	-2.3			2		1			2		
(-2.2) - (-2.0)	-2.1			1	2	1	1	2		1	1
(-2.0) - (-1.8)	-1.9		1	2	1	1	1	3	3		1
(-1.8) - (-1.6)	-1.7		2	2	1	3		3	1	1	
(-1.6) - (-1.4)	-1.5	1	3	5	3	2		1	2		
(-1.4) - (-1.2)	-1.3		3	1	2	2		1	1	1	
(-1.2) - (-1.0)	-1.1	5	5	5	3	2	3	2	1		
(-1.0) - (-0.8)	-0.9	2	8	5	4	2	1	3	2	1	
(-0.8) - (-0.6)	-0.7	5	15	10	2	2	1		1		1
(-0.6) - (-0.4)	-0.5	4	5	8	3		1				
(-0.4) - (-0.2)	-0.3	10	17	7	4	3					
(-0.2) - (0.0)	-0.1	13	23	8	4	2					
(0.0) - (+0.2)	+0.1	15	25	5	2						
	total	55	107	61	31	22	9	15	13	4	3
	< z > (kpc)	0.75	1.37	2.41	3.57	4.50	5.53	6.42	7.42	8.30	9.75
	$<[Fe/H]>(\mathrm{dex})$	-0.31	-0.41	-0.76	-0.84	-1.19	-1.32	-1.51	-1.53	1.50	-1.30
	m.e.	±0.16	±0.25	± 0.18	±0.12	±0.10	±0.10	±0.19	±0.16	±0.09	±0.08

eters. We now review our results and discuss them in the context of those by other authors.

(i) The use of colour data to identify and reject extragalactic objects.

A considerable fraction of the star candidates of Hall et al. (1996), selected from image structure, and labelled with "s", "sf", and "Fs" in their work turned out to be extra-galactic objects, according to their position in the $(U-B)_o$ - $(B-V)_o$ colour-colour diagram. An effective colour cut, consistent with those adopted by SDSS (Chen et al. 2001) is to reject all point-sources with $(U-B)_o$ colour indices less than -0.46, which corresponds to $(u'-g')_o < -0.50$. Comparison of Fig.1 and Fig.2 shows that this single selection substantially reduces scatter away from the stellar locus. Removal of objects with $(U-B)_o < -0.46$ and imposing an apparent magnitude cut at the completeness limit $V_o \leq 20.5$ allowed the stellar locus to be readily identified, and outliers to be excluded.

(ii) Stellar luminosity function at r=0 kpc obtained from deep CCD-photometry.

The sample of Hall et al. (1996) does not allow space density determination for nearby stars due to the lack of apparently bright stars in this sample. Hence, space densities are complete at distances larger than 2.51, 1.00, and 0.63 kpc for absolute magnitude intervals $4 < M(V) \le 5$, $5 < M(V) \le 6$, and $6 < M(V) \le 7$, respectively, and 0.40 kpc for four absolutely fainter intervals, i.e.: $7 < M(V) \le 8$, $8 < M(V) \le 9$, $9 < M(V) \le 10$, and $10 < M(V) \le 11$.

In order to allow comparison with the local luminosity functions of Hipparcos (Jahreiss & Wielen 1997) and with that evaluated by Kul (1994) from the data of Gliese & Jahreiss (1992), the star count models themselves must be used to extrapolate the star counts to the solar neighbourhood. While in general all three models analysed are in tolerable agreement with the required local normalizations, there are differences. The model of Buser et al. fits best for three absolute magnitude intervals, i.e.: $6 < M(V) \le 7$, $8 < M(V) \le 9$, and $9 < M(V) \le 10$, relative to that of Gilmore & Wyse (Fig.9a). This difference is due to the differences between scale-heights and local densities adopted for the thick disk (cf Table 3). The model of Chen et al. matches the constraint well for low luminosity local thin disk stars, absolutely faint magnitude intervals (M(V) > 8) whereas the model of Buser et al. matches better for the more luminous thick disk stars, for the bright ones (M(V) < 7). This distinction is due to differences between five model parameters (Table 3). Additionally, one must take into account the difference density laws used for the halo for these models, i.e.: de Vauceuleurs spheroid for Buser et al., and power-law for Chen et al.

We determined the sensitivity of the local luminosity function constraint on determination of the axis ratio of the halo by calculating models following Chen et al. except with axis ratio $\eta=0.65$ (Fig.10a) and $\eta=0.84$ (Fig.10b). The first value (0.65) is that derived by Yanny et al. (2000) based on BHB tracers from *SDSS* data, and rather close to the value (0.6) suggested by Wyse & Gilmore (1988). The second value is not only equal or close to the values propesed by Buser et al. and Gilmore & Wyse, but also it coincides with those cited by other authors. For example Hawkins (1984), and Bahcall & Soneira (1984) found $\eta=0.9$, and $\eta=0.8$ respectively. Preston et al. (1991) state that η increases from 0.5 to 1 up

to 20 kpc, while Robin et al. (2000) deduced that the halo has a flattening of $\eta=0.76$. It is interesting that the luminosity function comparison in figures 10a and 10b distinguish these models, thus showing that the flattening parameter η of the halo is the most sensitive parameter which can be distinguished here between the Buser et al. and the Chen et al. models. Finally, a de Vaucouleurs spheroid with the model parameters of Chen et al., except that $\eta=0.84$, works well, (Fig.10c) indicating that η but not the density law for the halo plays an important role in the luminosity function comparison. Overall, we conclude that the model of Chen et al. (2001) is consistent with these data, under the condition that $\eta=0.84$.

(iii) Vertical metallicity gradient for the three components of the Galaxy

Our data are consistent with, but do not require, weak vertical metallicity gradients in both the thin disk and thick disk. In the halo, any vertical metallicity gradient is even weaker. A better description of our data is that the metallicity distribution function is the sum of three discrete distributions, none of which has a significant metallicity gradient. Rather, an apparent vertical metallicity gradient arises from the changing contributions of the three distributions with distance from the Galactic Plane. Some gradient inside each population is however allowed by our analysis.

The maximum possible vertical metallicity gradient for the thin disk, i.e.: $d[Fe/H]/dz \sim -0.2$ dex/kpc, is consistent with many other determinations, and consistent with a convolution of a weak age-metallicity relation and age-velocity dispersion relation.

If there were a detected vertical metallicity gradient for the thick disk this would impact some formation histories postulated for the formation of the classical thick disk. Until recently this component of our Galaxy was assumed to have a mean metalabundance $[Fe/H] \sim -0.60$ dex, with a narrow metallicity range, a scale-height 1.0-1.3 kpc, and that it comprises some 0.02-0.05of the material in the solar neighbourhood. Additionally, and more important, it was argued that the stars of thick disk were formed from a merger into the Galaxy (cf. Norris 1996 and references within), a formation mechanism unlikely to leave an abundance gradient. Some recent analyses suggested that the thick disk is a more massive component of the Galaxy, (Majewski 1993) with a metal-poor (Norris 1996) and a metal-rich tail (Carney 2000; Karaali et al. 2000). Hence, a revision of the formation scenario of the thick disk may be required. The work of Reid & Majewski (1993) in which a vertical metallicity gradient $d[Fe/H]/dz \sim$ -0.10 dex/kpc is claimed is consistent with our results (Fig.12) but also consistent with a simple no-gradient mixed-population model. Chiba & Yoshii (1998) also suggest a vertical metallicity gradient for the thick disk. A substantially larger sample of stars with both metallicities and appropriate kinematics will be required to distinguish between these models (cf Gilmore, Wyse, & Norris 2002).

Detection of a metallicity gradient in the halo which changes with Galactocentric distance would be a test of scenarios suggesting important late accretion of the outermost part of the Galaxy: One might expect a gradient in the inner partly-dissipatively formed halo, and none farther out, provided that the stellar velocity ellipsoid is as observed, only slightly radially anisotropic. This gradient is consistent with our results: i.e.: there is a slight vertical metallicity gradient, $d[Fe/H]/dz \sim -0.10$ dex/kpc, in the inner part of the halo (5 < $z \le 8$ kpc) and zero in its outer part (8 < $z \le 10$

kpc). However, we recognize that there are significant statistical uncertaintes and a proper interpretation will need to await large-scale stellar surveys from the *SDSS*.

ACKNOWLEDGMENTS

This work was supported by the Research Fund of the University of Istanbul. Project number 1417/050500. We thank to Hall et al. (1996) for providing their data.

REFERENCES

Ak, S.G., Karaali, S., & Buser, R., 1998, A&AS, 131, 345

Bahcall, J.N., & Soneira, R.M., 1984, ApJS, 55, 67

Bahcall, J.N., 1986, ARAA, 24, 577

Becker, W., 1965, ZA, 62, 54

Beers, T.C., & Sommer-Larsen, J., 1995, ApJS, 96, 175

Buser, R., Rong, J., & Karaali, S., 1998, A&A, 331, 934 (BRK)

Buser, R., Rong, J., & Karaali, S., 1999, A&A, 348, 98 (BRK)

Carney, B.W., Latham, D.W., & Laird, J.B., 1990, AJ, 99, 572

Carney, B.W., 2000, Proceedings of the 35^{th} Liége Int. Astrophys. Coll., July 5-8, 1999, p. 287

Cayrel de Strobel, G., Soubiran, C., Friel, E. D., Ralite, N., & Francois, P., 1997, A&AS, 124, 299

Cayrel de Strobel, G., Soubiran, C., & Ralite, N., 2001, A&A, 373, 159

Chen, B., Stoughton, C., Smith, J. A., Uomoto, A., Pier, J. R., Yanny, B., Ivezic, Z., York, D. G., Anderson, J. E., Annis, J., Brinkmann, J., Csabai, I. Fukugita, M., Hindsley, R., Lupton, R., Munn, J. A., and the SDSS Collaboration, 2001, ApJ, 553, 184 (C)

Chiba, M., & Yoshii, Y., 1998, AJ, 115, 168

Del Rio, G., & Fenkart, R.P., 1987, A&AS, 68, 397

Eggen, O. J., Lynden-Bell, D., & Sandage A.R., 1962, ApJ, 136, 748 (ELS)

Fenkart, R.P., & Karaali, S., 1987, A&AS, 69, 33

Fenkart, R.P., 1989a, A&AS, 78, 217

Fenkart, R.P., 1989b, A&AS, 79, 51

Fenkart, R.P., 1989c, A&AS, 80, 89

Fenkart, R.P., 1989d, A&AS, 81, 187

Fenkart, R.P., & Karaali, S., 1990, A&AS, 83, 481

Fenkart, R.P., & Karaali, S., 1991, A&AS, 88, 233

Freeman, K., Bland-Hawthorn, J., 2002, ARA&A, 40, 487

Gilmore, G., & Wyse, R.F.G., 1985, AJ, 90, 2015 (GW)

Cilinary C. Wass D.E.C. & Walliam V. 1000 ADA & A

Gilmore, G., Wyse, R.F.G., & Kuijken, K., 1989, ARA&A, 27, 555

Gilmore, G., 2000, JBAA 110, 42

Gilmore, G., Wyse, R.F.G., & Norris, J.E., 2002, ApJ, 574, 39

Gliese, W., & Jahreiss, H., 1992, Third Catalogue of Nearby Stars (Preliminary Version), Astron. Rechen Inst. Heidelberg

Hall, P.B., Osmer, P.S., Green, R.F., Porter, A.C., & Warren, S.J., 1996, ApJS, 104, 185

Hawkins, M.R.S., 1984, MNRAS, 206, 433

Hesser, J.E., Harris, W.E., Vandenberg, D.A., Allwright, J.W.B., Shott, P., & Stetson, P.B., 1987, PASP, 99, 739

Jahreiss, H., & Wielen, R., 1997, in: HIPPARCOS'97. Presentation of the HIPPARCOS and TYCHO catalogues and first astrophysical results of the Hipparcos space astrometry mission., Battrick, B., Perryman, M.A.C., & Bernacca, P.L., (eds.), ESA SP-402, Noordwyk, p.675

Johnson, R.A., Gilmore, G., Tanvir, N.R., & Elson, R.A.W., 1999, NewA, 4, 431

Karaali, S., Karataş, Y., Bilir, S., Ak, S.G., & Gilmore, G.F. 2000, Proceedings of the 35th Liége Int. Astrophys. Coll., July 5-8, 1999, p.353

Karaali, S., Bilir, S., Karataş, Y., & Ak, S.G., 2002, PASA (accepted) Karataş, Y., Karaali, S., & Buser, R., 2001, A&A, 373, 895

Kul, F., 1994, Master Thesis, University of Istanbul, Institute of Advance Studies, Istanbul

Lang, K.R., 1992, Astrophysical Data I. Planets and Stars, Berlin, Springer-Verlag

Figure A1. The third-degree polynomial curve throught 17 locus-points and the correlation coefficient. The bars show the mean errors.

Majewski, S.R., 1993, ARA&A, 31, 575

Mermilliod, J. C., Mermilliod, M., Hauck, B., 1997, A&AS, 124, 349

Norris, J.E., Bessell, M.S., & Pickles, A.J., 1985, ApJS, 58, 463 (NBP)

Norris, J.E., 1986, ApJS, 61, 667

Norris, J.E., 1996, ASP Conf. Ser. Vol. 92, p.14, Eds. H.L. Morrison & A.Saraiedini

Norris, J.E., & Ryan, S.G., 1991, ApJ, 380, 403

Phleps, S., Meisenheimer, K., Fuchs, B., & Wolf, C., 2000, A&A, 356, 108

Preston, G.W., Shectman, S.A., & Beers, T.C., 1991, ApJS, 76, 1001

Preston, G.W., & Sneden, C., 2000, AJ, 120, 1014

Reid, N., & Majewski, S.R., 1993, ApJ, 409, 635

Richer, H.B., & Fahlman, G.G., 1986, ApJ, 304, 273

Robin, A.C., Reylé, C., & Crézé, M., 2000, A&A, 359, 103

Rosenberg, A., Saviane, I., Piotto, G., & Aparicio, A., 1999, AJ, 118, 2306

Sandage, A., & Fouts, G., 1987, AJ, 93, 74

Schuster, W.J., & Nissen, P.E., 1989, A&A, 222, 69

Searle, L., & Zinn, R., 1978, ApJ, 225, 357 (SZ) Stetson, P.B., & Harris, W.E., 1988, AJ, 96, 909

Unavane, M., Wyse, R.F.G. & Gilmore, G., 1996, MNRAS, 278, 727

Wyse, R.F.G., & Gilmore, G., 1988, AJ, 95, 1404

Willman, B., Dalcanton, J., Ivezic, Z., Jackson, T., Lupton, R., Brinkmann, J., Hennessy, G., & Hindsley, R., 2002, AJ, 123, 848

Yanny, B., Newberg, H.J., Kent, S., Laurent-Muehleisen, S.A., Pier, J.R., Richards, G.T., Stoughton, C., Anderson, J.E.Jr., Annis, J., Brinkmann, J., Chen, B., Csabai, I., Doi, M., Fukugita, M., Hennessy, G.S., Ivezic, Z., Knapp, G.R., Lupton, R., Munn, J.A., Nash, T., Rockosi, C.M., Schneider, D.P., Smith, J.A., & York, D.G., 2000, ApJ, 540, 825 Yoshii, Y., & Saio, H., 1979, PASJ, 31, 339

APPENDIX A: THE NEW METALLICITY CALIBRATION

Data for 88 dwarfs with metallicities $-2.7 \le [Fe/H] \le +0.26$ dex were taken from three sources for a new metallicity calibration: (1) 57 of them with $logg \ge 4.5$ are from Cayrel de Strobel et al. (2001), a catalogue which supplies detailed information for stars with abundance determinations based on high-resolution spectroscopy. (2) 11 high or intermediate mass stars were taken from a different catalogue of the same authors (Cayrel de Strobel et al. 1997). This catalogue has the advantage of including metalpoor stars down to [Fe/H] = -2.70 dex with smaller gravity, i.e.: $logg \ge 4.0$, however. For the *UBV*-magnitudes and colours, specialised catalogues which are included in the General Catalogue of Photometric Data (Mermilliod et al. 1997) were consulted. The parallax and the galactic latitude of stars which were used in the choice of the sample stars were provided from the database. (3) 20 stars classified as dwarfs by Carney (1979) who used them in his metallicity calibration were included also in the new sample.

The full interval for normalized ultra-violet excess, $-0.09 \le \delta_{0.6} \le +0.38$ mag was divided into 17 sub-intervals. The centroid of each was adopted as a locus point to fit the couple $(\delta_{0.6}, [Fe/H])$. Table A1 gives the locus points and the number of stars associated, and Fig.A1 the fit of these points by a third-degree polynomial, i.e.: $[Fe/H] = 0.10 - 2.76\delta - 24.04\delta^2 + 30.00\delta^3$. Analysis of the deviations of metallicities deduced from this calibration compared to the original metallicity shows that the accuracy is at the level of Carney (1979)'s work (Fig.A2a-c).

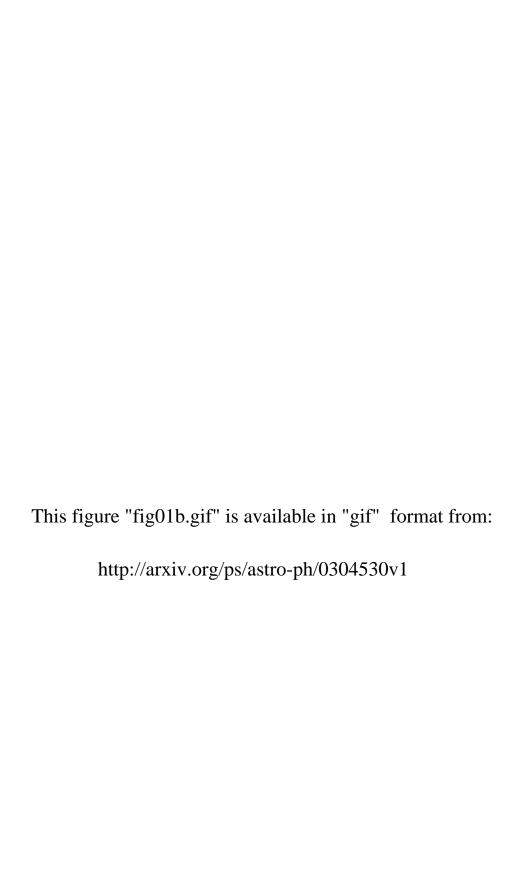
This paper has been produced using the Royal Astronomical Society/Blackwell Science LATeX style file.

Table A1. Locus points and the number of stars associated with them (last column). The other colums give the current number, $\delta_{0.6}$, [Fe/H], mean errors for the $\delta_{0.6}$ and [Fe/H] and, respectively.

No	$\delta_{0.6}$	[Fe/H]	$\Delta \delta_{0.6}$	$\Delta [Fe/H]$	N
1	-0.07	+0.21	0.01	0.04	3
2	-0.02	+0.09	0.00	0.04	8
3	+0.01	+0.05	0.00	0.02	7
4	+0.02	+0.01	0.00	0.04	7
5	+0.04	-0.04	0.00	0.03	7
6	+0.08	-0.28	0.00	0.03	8
7	+0.11	-0.41	0.00	0.03	7
8	+0.14	-0.62	0.00	0.04	8
9	+0.15	-0.75	0.00	0.03	5
10	+0.17	-0.93	0.00	0.04	4
11	+0.19	-1.05	0.00	0.07	3
12	+0.22	-1.32	0.00	0.04	5
13	+0.23	-1.52	0.00	0.06	3
14	+0.26	-1.68	0.00	0.03	3
15	+0.28	-2.05	0.00	0.06	4
16	+0.31	-2.10	0.00	0.04	3
17	+0.36	-2.60	0.01	0.05	3

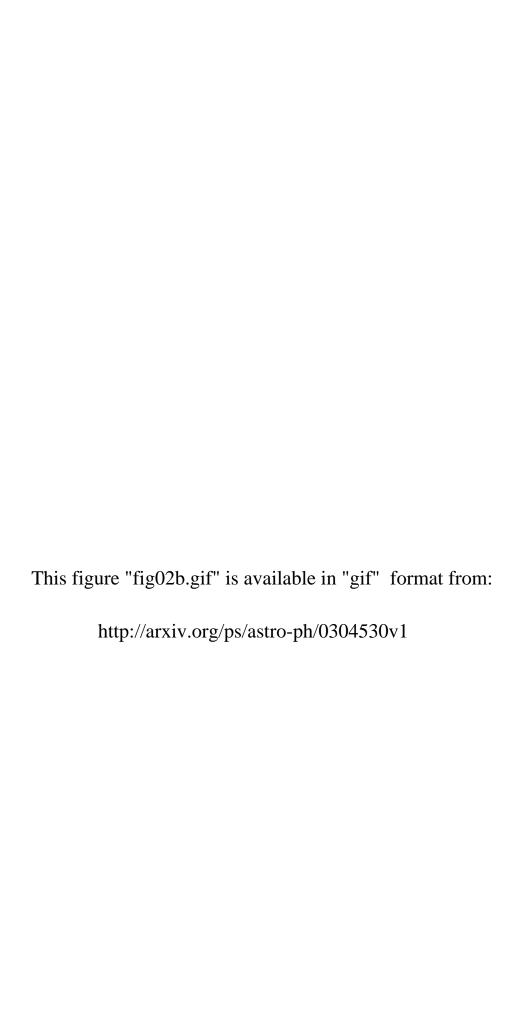
Figure A2. Deviation of evaluated metallicities from original ones versus original metallicity for all stars in our sample (a), for stars with $\lceil Fe/H \rceil \ge -1.75$ dex in our sample (b), and for the sample of Carney (c), where $\lceil Fe/H \rceil = -1.75$ dex is the validity limit for the Carney (1979) calibration.

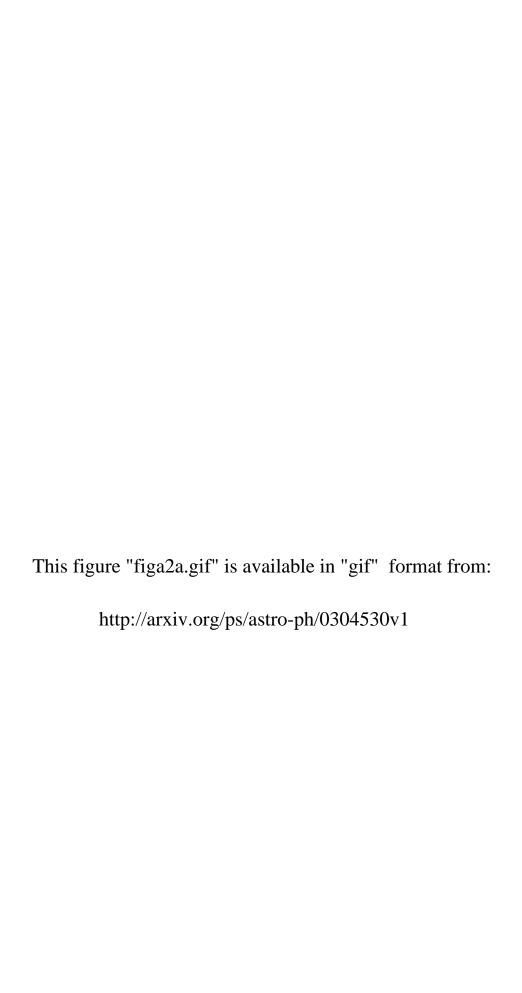
This figure "fig01a.gif" is available in "gif" format from:

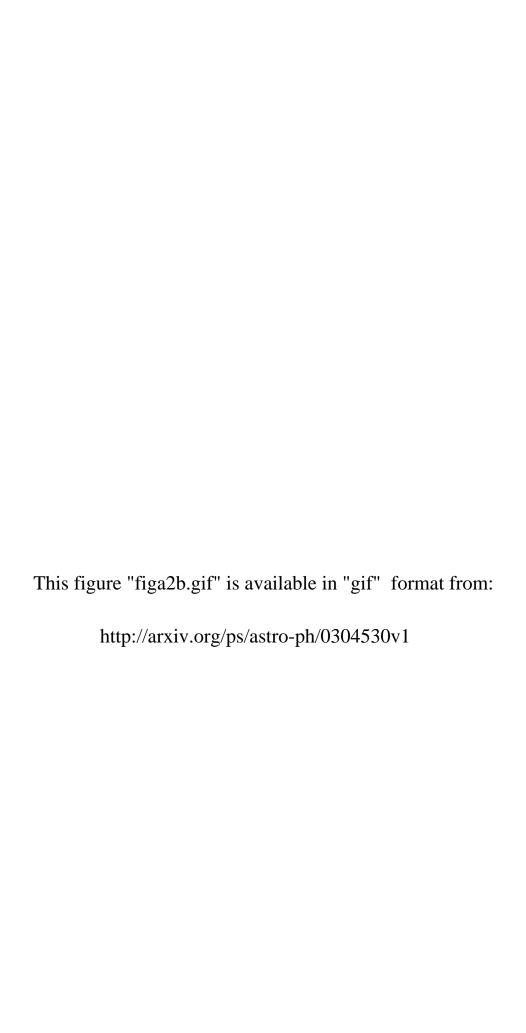


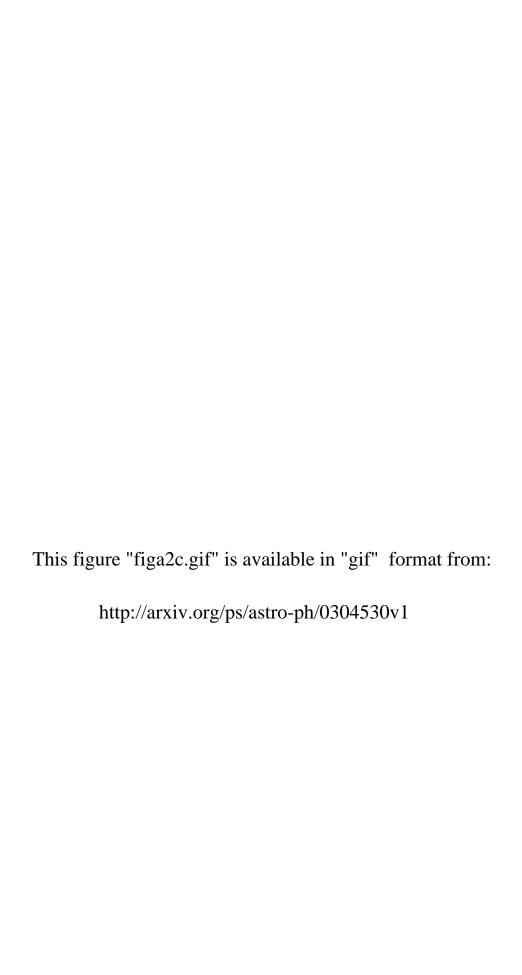
This figure "figa1.gif" is available in "gif" format from: http://arxiv.org/ps/astro-ph/0304530v1

This figure "fig02a.gif" is available in "gif" format from: http://arxiv.org/ps/astro-ph/0304530v1

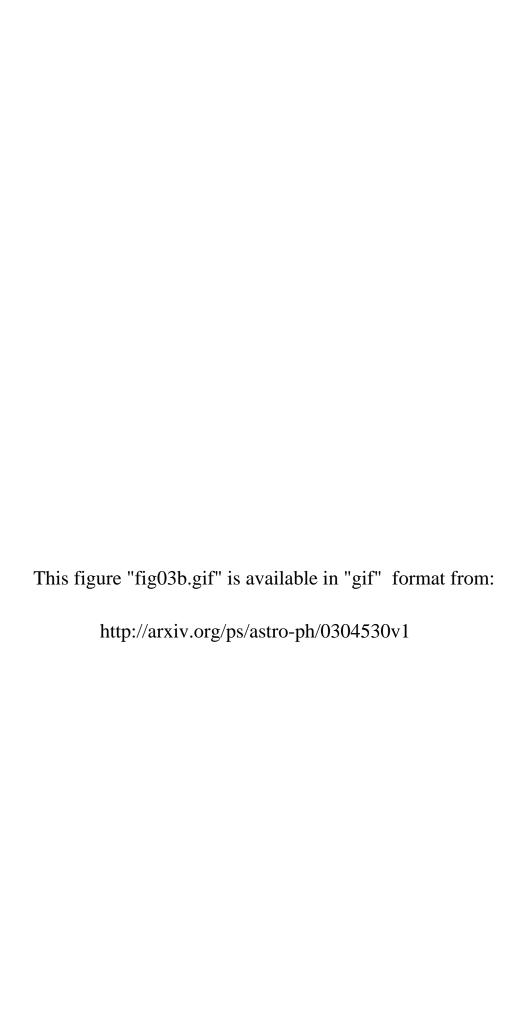






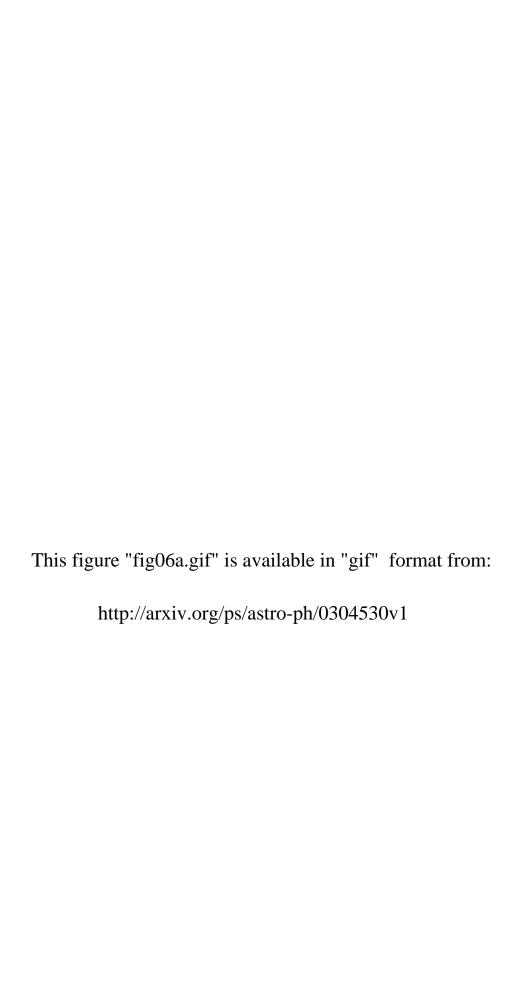


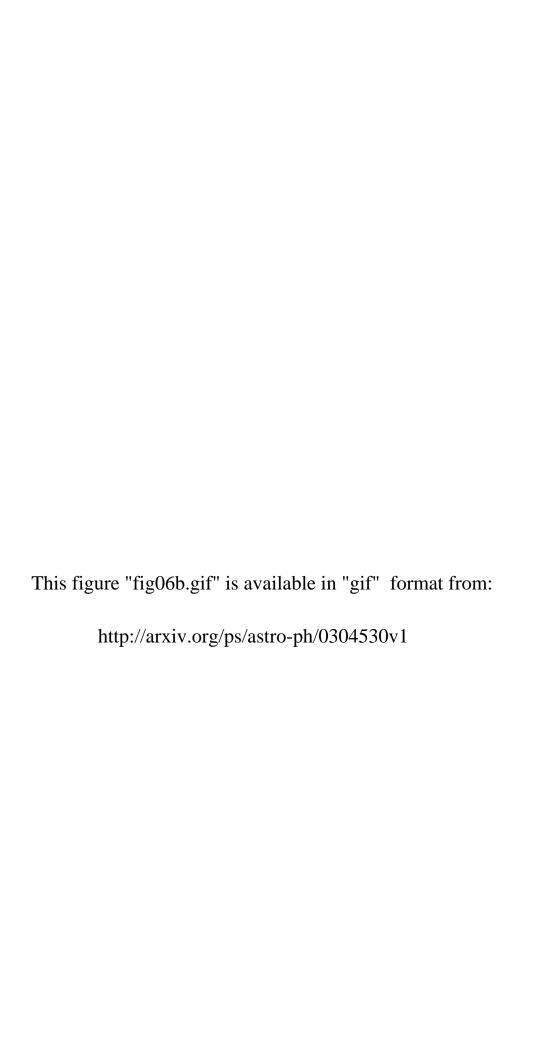
This figure "fig03a.gif" is available in "gif" format from: http://arxiv.org/ps/astro-ph/0304530v1

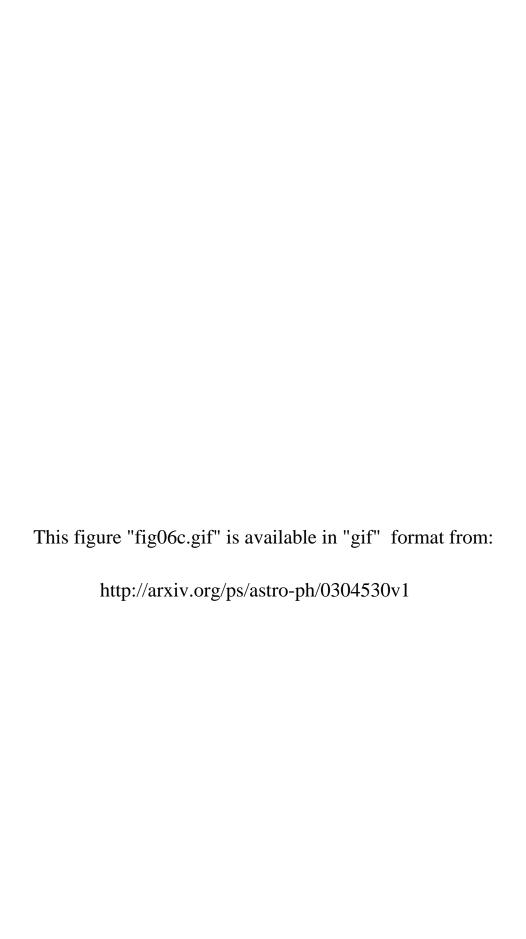


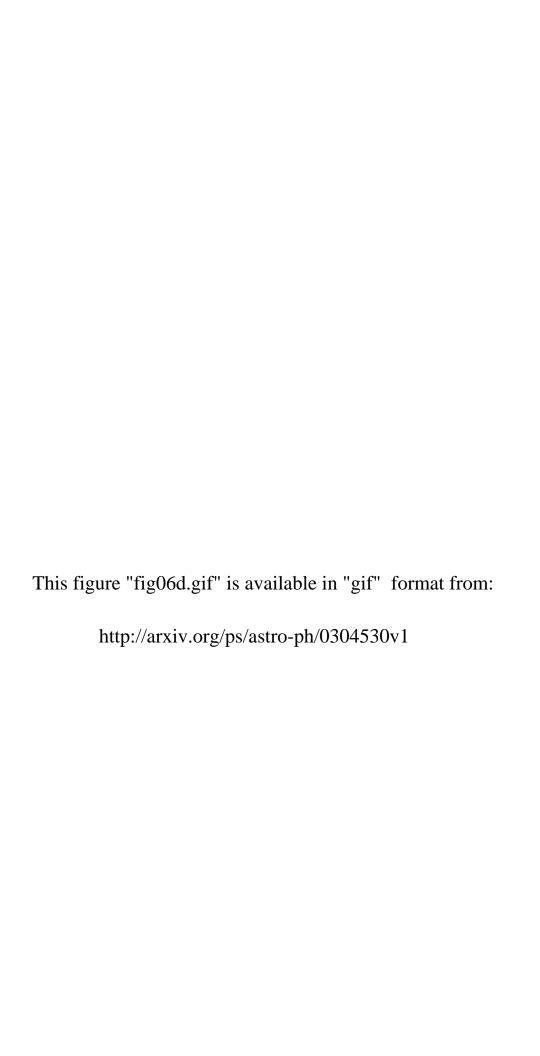
This figure "fig04.gif" is available in "gif" format from:

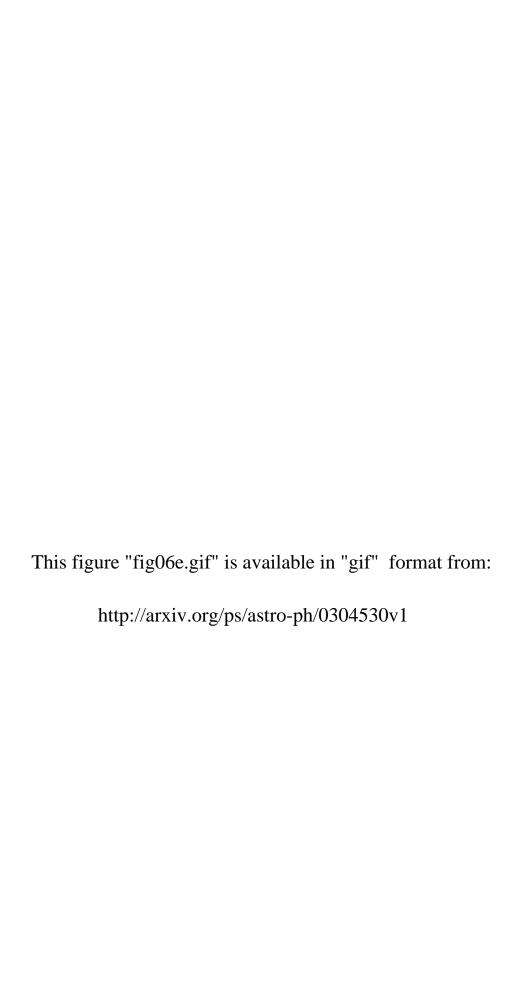
This figure "fig05.gif" is available in "gif" format from:

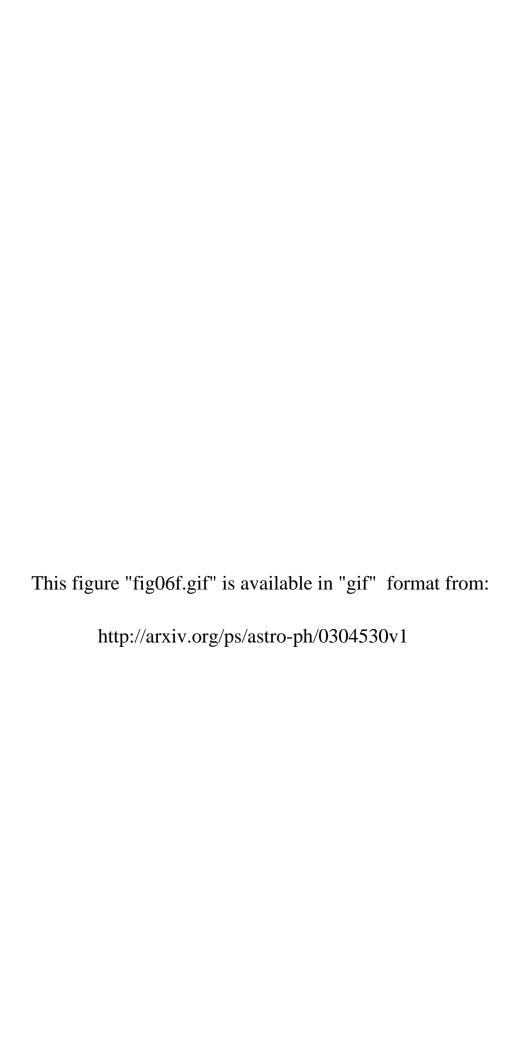




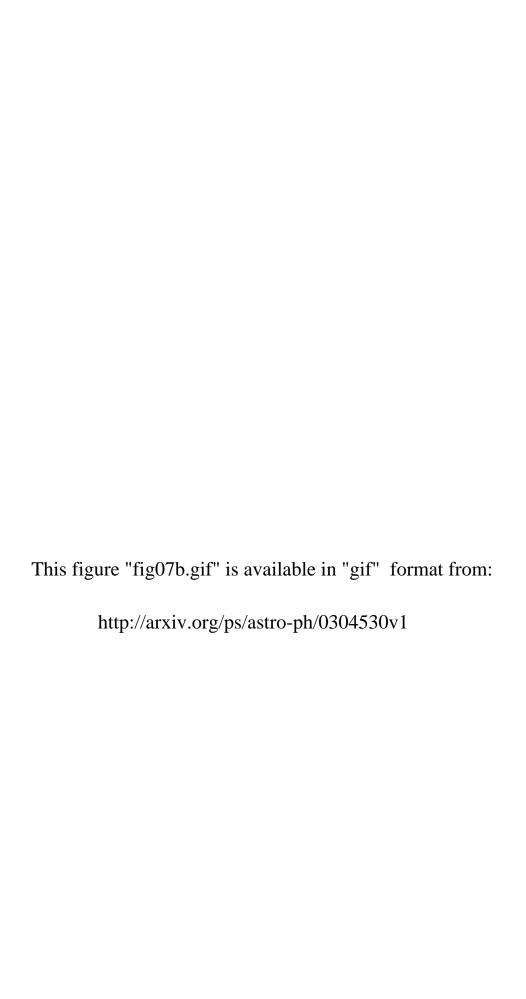




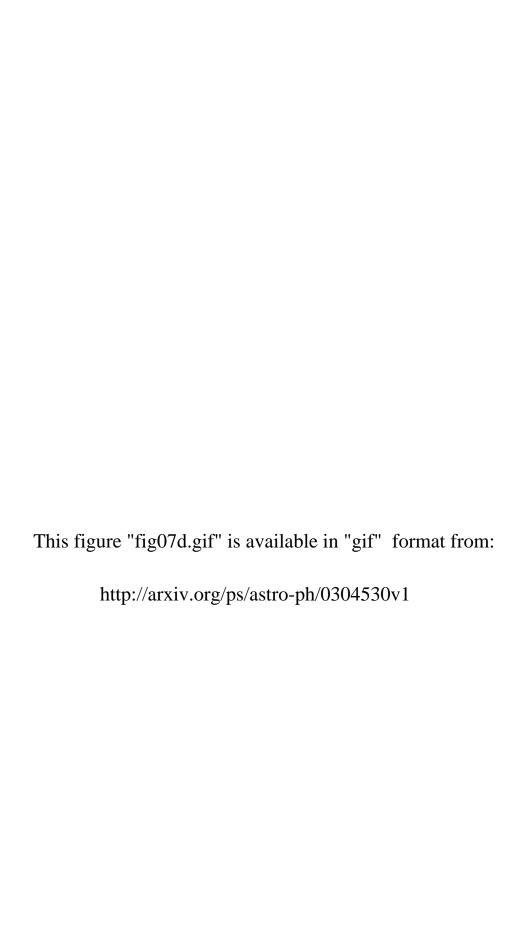


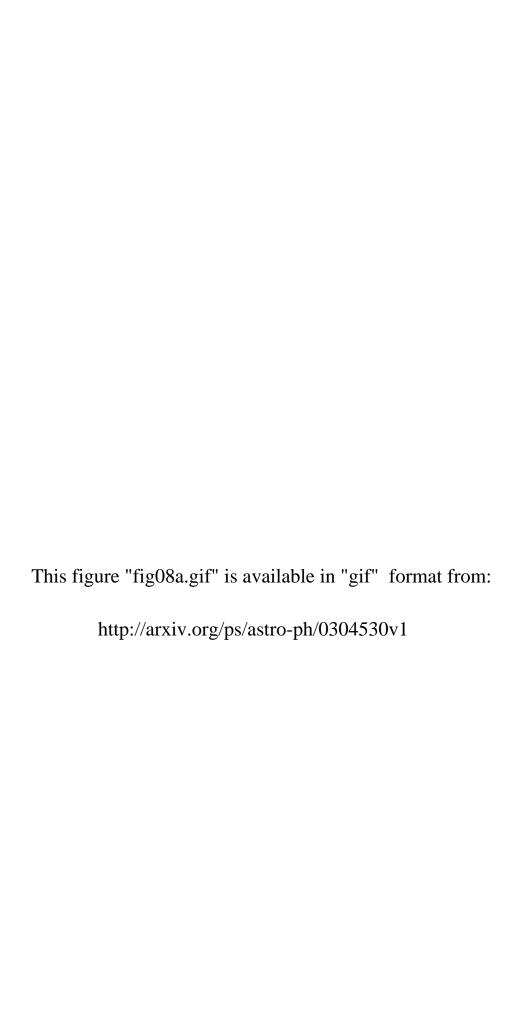


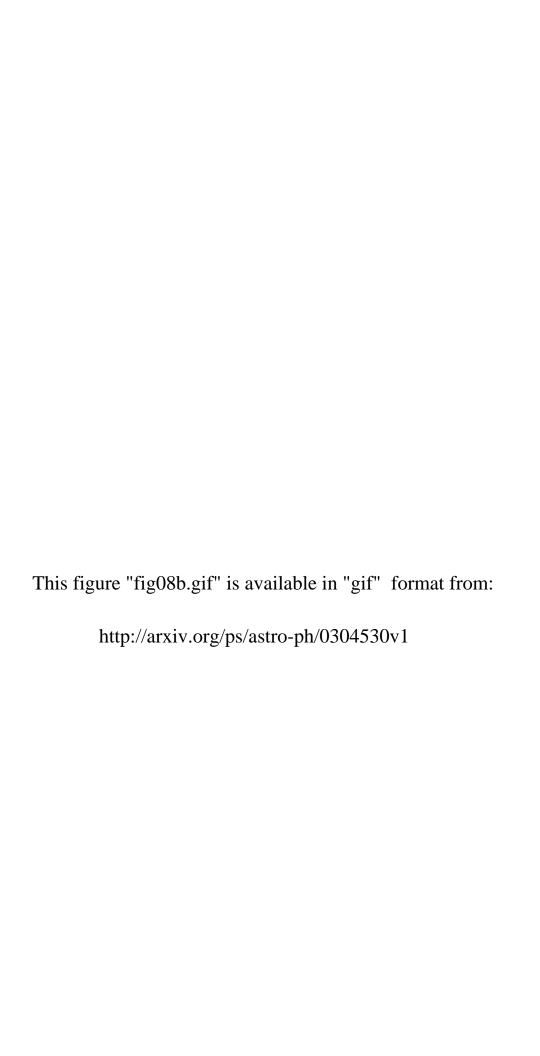
This figure "fig07a.gif" is available in "gif" format from:

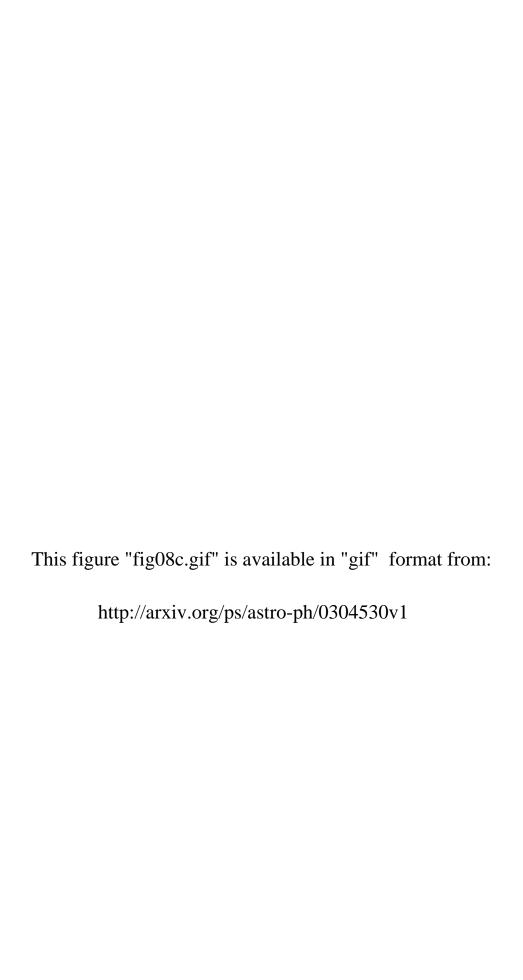


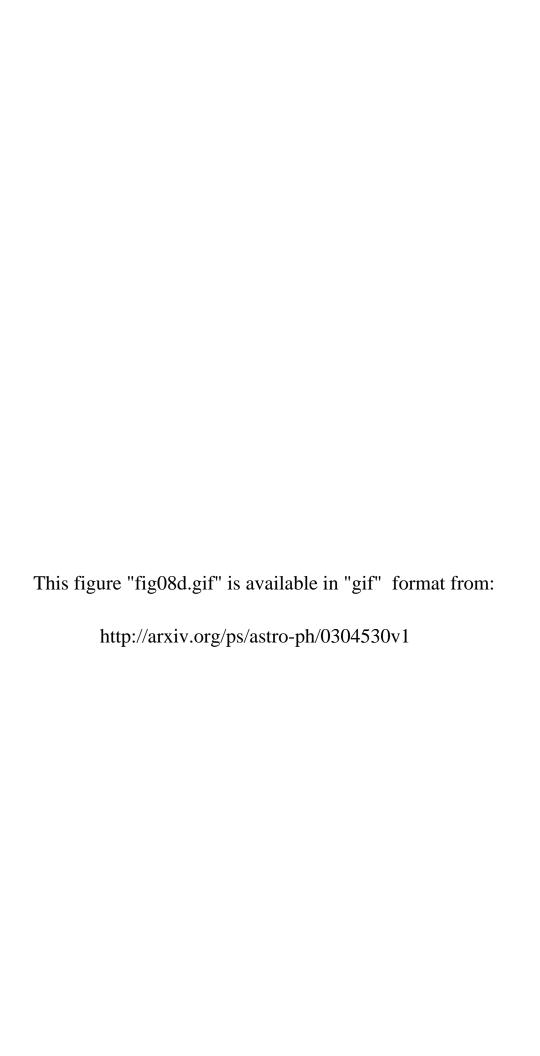
This figure "fig07c.gif" is available in "gif" format from: http://arxiv.org/ps/astro-ph/0304530v1

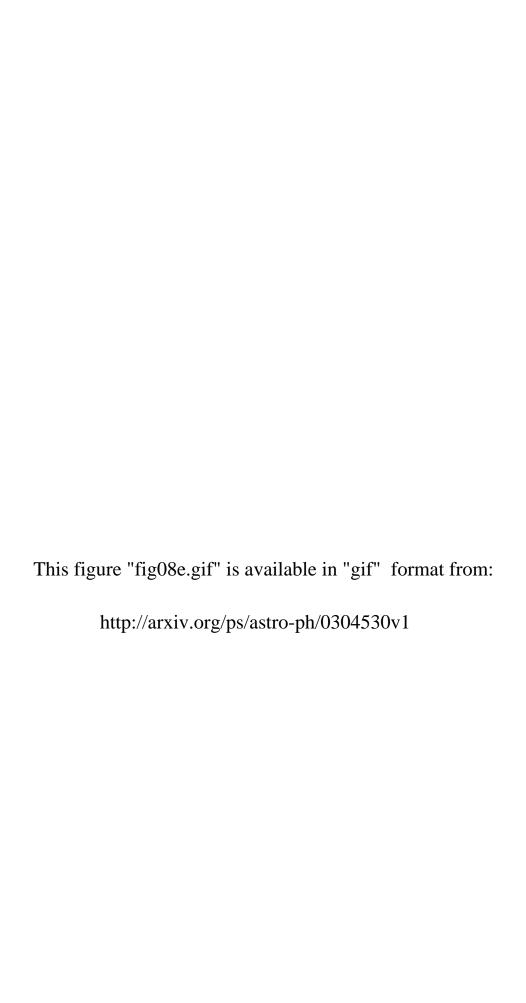


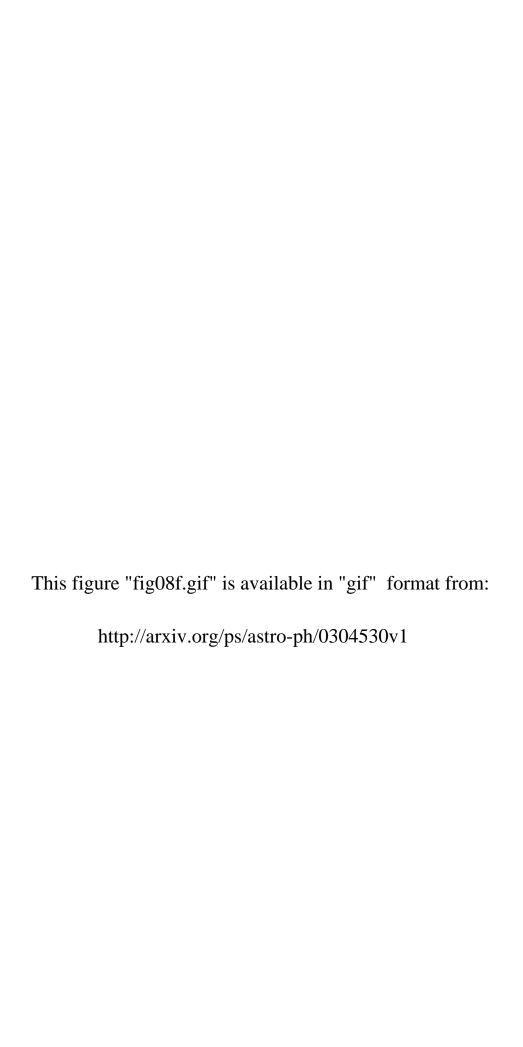


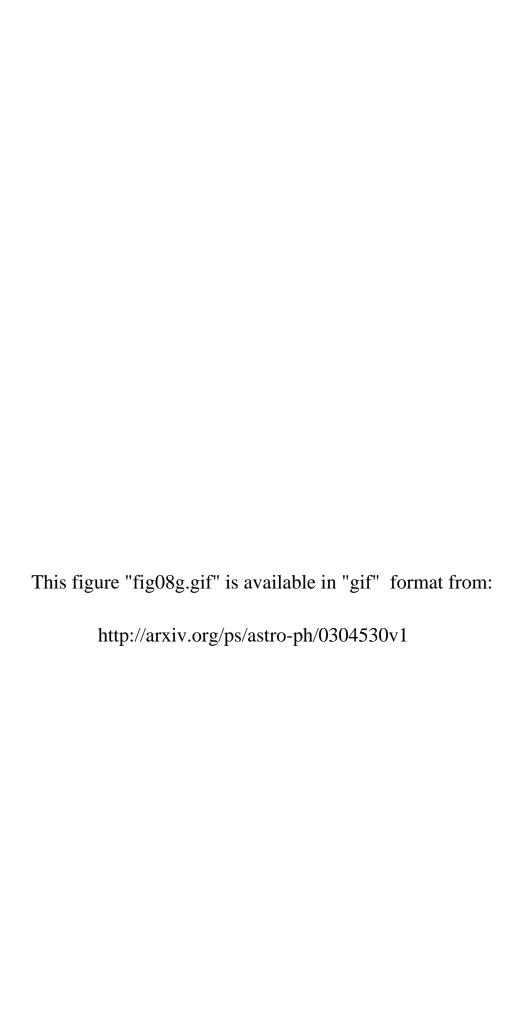


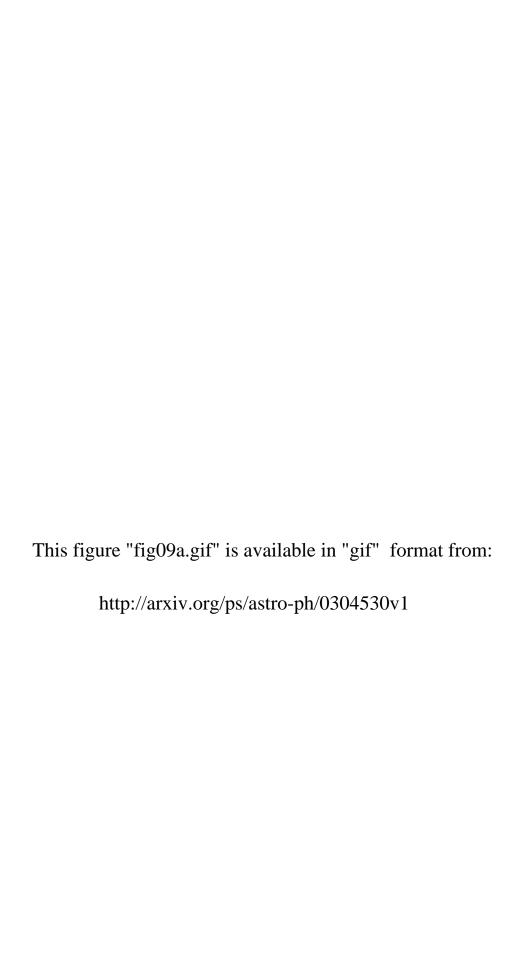


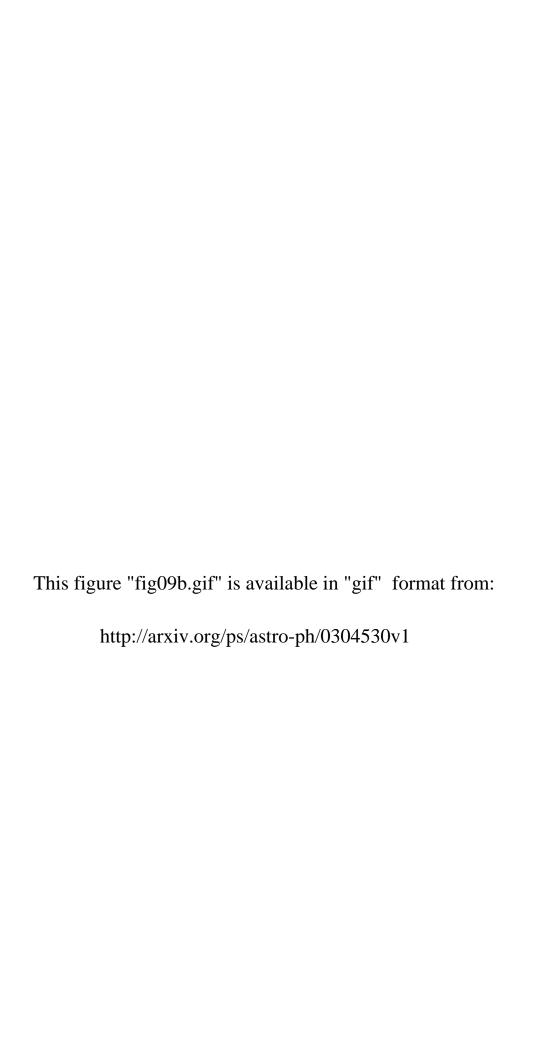


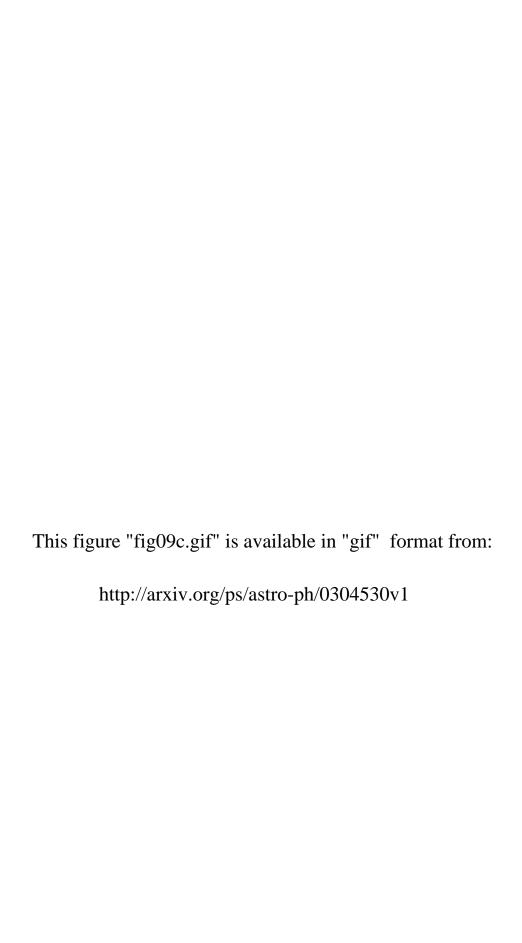


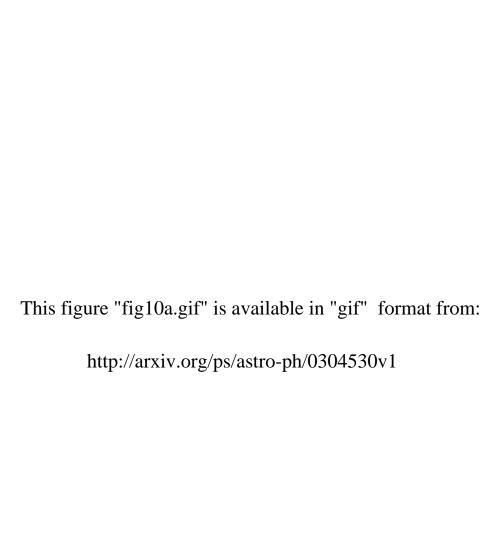


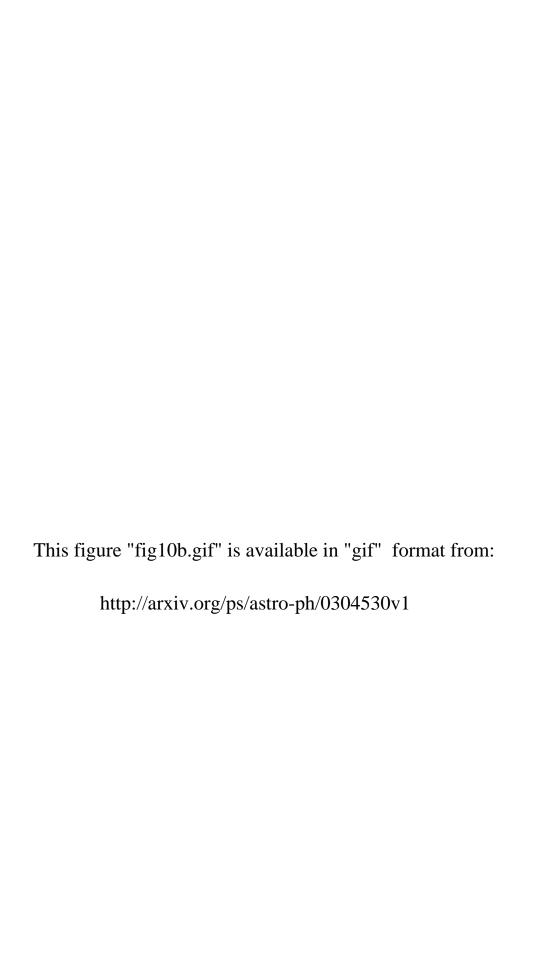




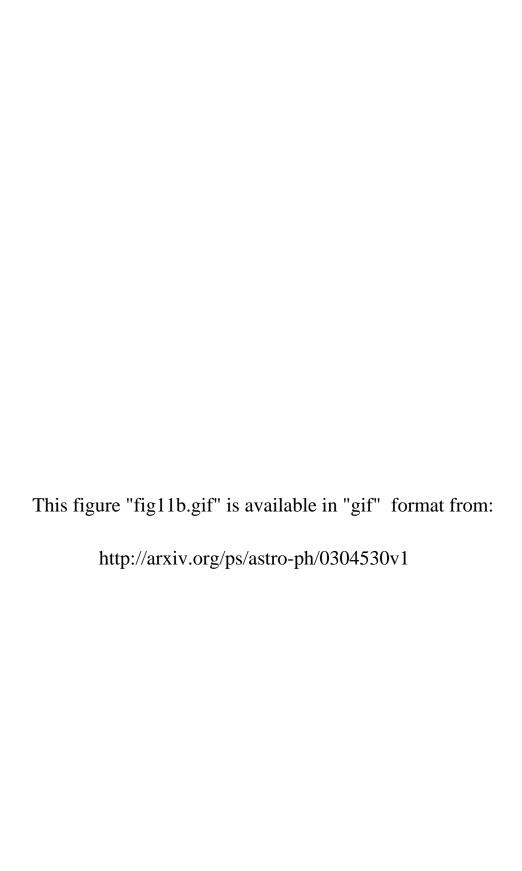








This figure "fig10c.gif" is available in "gif" format from: http://arxiv.org/ps/astro-ph/0304530v1 This figure "fig11a.gif" is available in "gif" format from: http://arxiv.org/ps/astro-ph/0304530v1



This figure "fig11c.gif" is available in "gif" format from: http://arxiv.org/ps/astro-ph/0304530v1 This figure "fig11d.gif" is available in "gif" format from: http://arxiv.org/ps/astro-ph/0304530v1

This figure "fig11e.gif" is available in "gif" format from: http://arxiv.org/ps/astro-ph/0304530v1

This figure "fig11f.gif" is available in "gif" format from:

http://arxiv.org/ps/astro-ph/0304530v1

This figure "fig11g.gif" is available in "gif" format from:

http://arxiv.org/ps/astro-ph/0304530v1

This figure "fig12.gif" is available in "gif" format from:

http://arxiv.org/ps/astro-ph/0304530v1